Journal of Sound and Vibration (1999) **219**(5), 905–919
Article No. jsvi.1998.1912, available online at http://www.idealibrary.com on IDEAL

LETTERS TO THE EDITOR

DYNAMIC ANALYSIS OF MULTI-MESH COUNTER-SHAFT TRANSMISSION

T. C. Lim

Department of Mechanical Engineering, *P.O. Box* 870276,
The University of Alabama, *Tuscaloosa*, *AL* 35487-0276, *U.S.A.*

AND

J. Li

Center for Automotive Research, *The Ohio State University*, 930 *Kinnear Road*,
Columbus, *OH* 43212, *U.S.A.*

(*Received* 8 *January* 1998, *and in final form* 31 *July* 1998)

1. INTRODUCTION

Analytical dynamic modelling of universal multi-mesh geared rotor systems is still quite scarce, even though the theory of single-mesh cylindrical gear pair vibration is extensively studied and well established. Most of these models depend on the basic lumped parameter vectorial formulation to represent the macro behavior of gear mesh kinematics. The method is quite reliable as evident from recent comprehensive literature reviews conducted by Ozguven and Houser [1], and Blankenship and Singh [2]. To address the lack of multi-mesh gear dynamic analytical work, this communication is concerned with the development of a generic n-mesh counter-shaft geared rotor system model.

Some of the original attempts to investigate the multi-mesh geared rotor system dynamic problem were by Iida *et al*. [3–5]. They analyzed the effects of translational and torsional motions of counter-shafts in dual-mesh systems. However, their analytical formulation is limited to spur gears and only the torsional degrees of freedom (DOF) of the input and output gears are modelled. Lim and Houser [6] also developed a dual-mesh counter-shaft model using a gear representation of 3 orthogonal translational displacements and a single torsional co-ordinate. A more rigorous rigid body gear model with 6 DOF was used by Kahraman [7] to analyze dual-mesh idler gear systems that do not contain a counter-shaft component. The most detailed dual-mesh model yet was established by Vinayak *et al*. [8, 9] to examine geared systems containing a single counter-shaft or idler gear. It incorporates a spatially distributed mesh stiffness formulation proposed by Blankenship and Singh in an earlier paper [10]. Other related studies of single counter-shaft problems include applications of the Ritz-based finite element technique by Velex and Saada [11], and a modal synthesis approach by Choy *et al*. [12]. Published experimental study involving counter-shaft transmission is even much scarcer. The most elaborate known was conducted by Umezawa *et al*. [13], which consists of numerous experiments to evaluate the effects of shaft length, input torque, and tooth mesh phase leg on dynamic

0022–460X/99/050905 + 15 $30.00/0

response. Some of the relevant experimental data is used here to validate our proposed theory.

As previous research efforts were confined to either the single or dual-mesh geared rotor system, it is the aim of this note to propose a set of generic analytical equations to describe the dynamics of a generalized multi-mesh geared system that consists of precisely n-sets of gear pairs and $n-1$ counter-shafts. This model incorporates the complete set of 3 translational and 3 rotational co-ordinates of each rigid gear structure with compliant mesh. The resulting linearized lumped parameter model is not only comprehensive, but also computationally efficient. It is applied as a suitable vibration analysis tool for evaluating preliminary design concepts, and computing the effects of assorted layouts and structural modifications on gear dynamic response. Our theory is validated by direct comparison to published experimental data [13] and numerical results of a finite element model for a specific $n=2$ case. In addition, a system with $n=3$ configuration is also analyzed to illustrate the effectiveness of this model.

2. FORMULATION

Consider a generic n-mesh flexible or quasi-rigid counter-shaft transmission system as illustrated in Figure 1. The pinion and gear of the second and higher mesh may assume an oblique orientation relative to a fixed inertial frame defined by the X, Y and Z axes. The X-axis is parallel to the mean rotational vector while the Y-axis passes through the geometric centers of the pinion and gear of the first mesh. Each gear pair could be either spur or helical type, and is completely defined

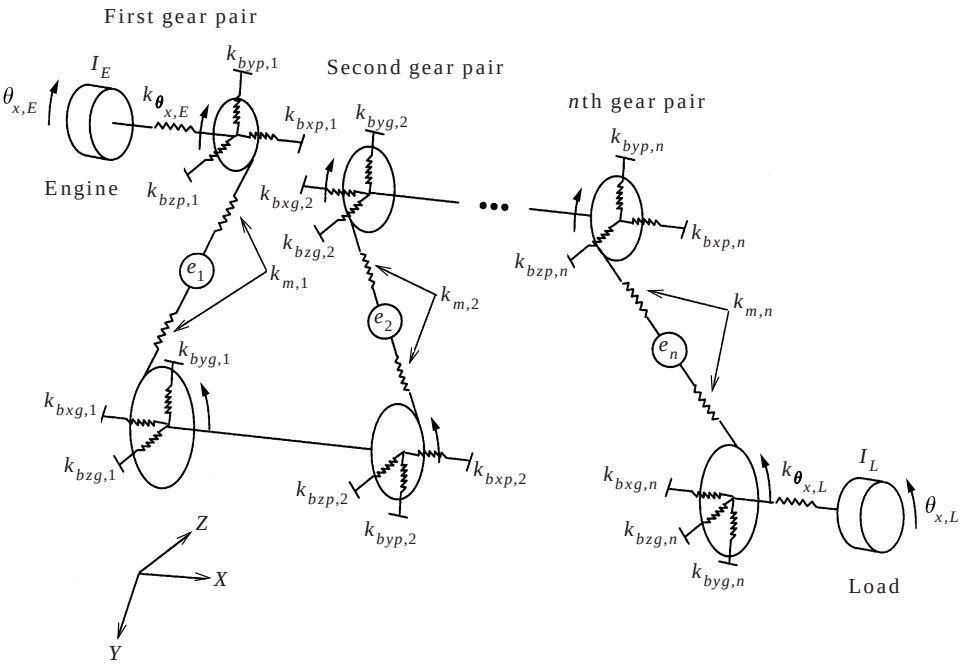

Figure 1. Elements of a n-mesh counter-shaft geared rotor system.

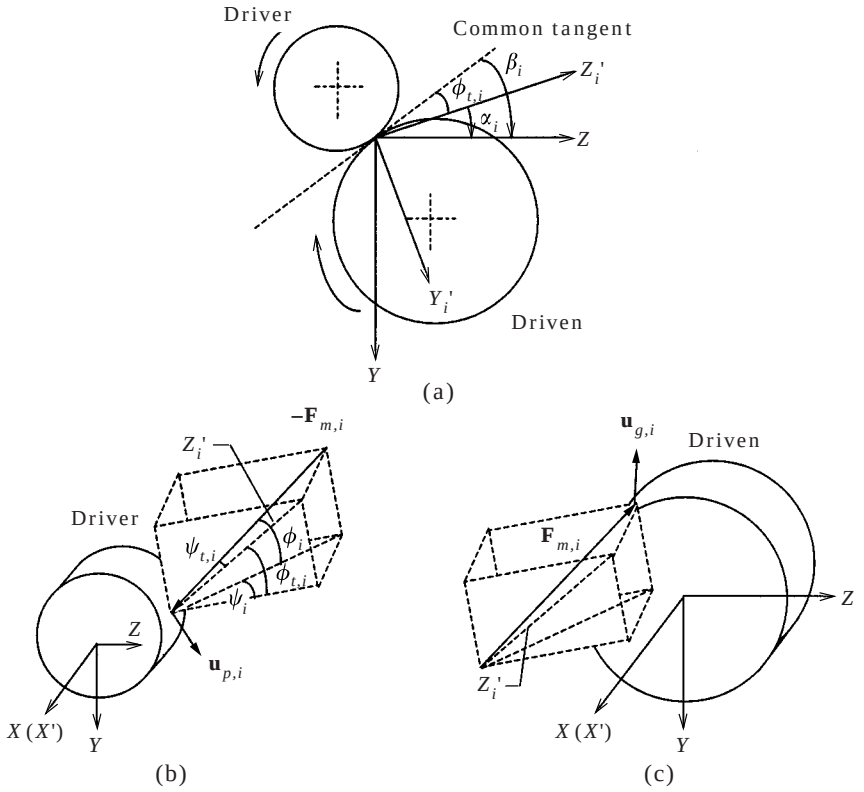

Figure 2. Mesh force and response vector in local (*prime*) and global (fixed) co-ordinate systems: (a) gear mesh orientation angles, (b) pinion (driver) component, (c) gear (driven) component.

by a generalized displacement vector of dimension 6 that comprises 3 translational and 3 rotational co-ordinates. Thus, an entire n-mesh system contains a total of $12n + 2$ co-ordinates.

Since each gear pair and counter-shaft assembly possesses similar features it can be formulated generically by considering a local *prime* co-ordinate system defined by X_i', Y_i' and Z_i' for the ith mesh, as shown in Figure 2. Here X_i' is parallel to X, Y_i' is perpendicular to Z_i', and Z_i' is the projection of $\mathbf{F}_{m,i}$ onto the Y–Z plane. The specific orientation of $\mathbf{F}_{m,i}$ is determined by the pressure angle ϕ_i, relative position angle β_i of pinion and gear, and mean rotational direction of the ith pair. To ensure that our derivation is general, the following sign convention is adopted: (1) $\phi_i > 0$, regardless of rotational direction; (2) helix angle ψ_i of driving pinion is positive if it is right-handed type, and negative if it is left-handed one; (3) β_i is positive when it is measured from the common tangent line to the Z-axis in the clockwise sense; (4) $\beta_1 = 0$.

Furthermore, a new set of geometrical and design angles are defined for convenience as

$$\phi_{t,i} = \tan^{-1}\left(\frac{\tan\phi_i}{\cos\psi_i}\right), \qquad 0 \leqslant \phi_{t,i} \leqslant \frac{\pi}{2}, \tag{1a}$$

$$\psi_{t,i} = \sin^{-1}(\cos\phi_i \sin\psi_i), \qquad \frac{-\pi}{2} \leqslant \psi_{t,i} \leqslant \frac{\pi}{2}, \tag{1b}$$

$$\alpha_i = \begin{cases} \pi + \beta_i + \phi_{t,i}, & \text{clockwise rotation of pinion } \theta_x^+, \\ \beta_i - \phi_{t,i}, & \text{counter-clockwise rotation of pinion } \theta_x^-, \end{cases} \tag{1c}$$

where $\phi_{t,i}$ is typically called the transverse pressure angle, $\psi_{t,i}$ is similar to a helix angle except it is measured in an oblique plane defined by $\phi_{t,i}$, and α_i is the gear mesh orientation angle used to relate the *prime* system to the fixed inertia frame.

The multi-dimensional undamped equations of motion of an arbitrarily positioned ith gear pair structure for both clockwise and counter-clockwise rotating pinions with respect to the displacement vectors $\mathbf{u}_{v,i} = \{u_{xv,i}, u_{yv,i}, u_{zv,i}, \theta_{xv,i}, \theta_{yv,i}, \theta_{zv,i}\}^{\mathrm{T}}$, $v = p$ or g (as shown in Figure 2), are given by

$$m_{v,i}\ddot{u}_{xv,i} - \varepsilon\gamma_i k_{m,i}\delta_i \sin\psi_{t,i} + k_{bxv,i}u_{xv,i} = 0, \tag{2a}$$

$$m_{v,i}\ddot{u}_{yv,i} + \varepsilon k_{m,i}\delta_i \cos\psi_{t,i} \sin\alpha_i + k_{byv,i}u_{yv,i} = 0, \tag{2b}$$

$$m_{v,i}\ddot{u}_{zv,i} - \varepsilon k_{m,i}\delta_i \cos\psi_{t,i} \cos\alpha_i + k_{bzv,i}u_{zv,i} = 0, \tag{2c}$$

$$I_{xv,i}\ddot{\theta}_{xv,i} + \gamma_i r_{v,i} k_{m,i}\delta_i \cos\psi_{t,i} \cos\phi_{t,i} = 0, \tag{2d}$$

$$I_{yv,i}\ddot{\theta}_{yv,i} - \gamma_i r_{v,i} k_{m,i}\delta_i \sin\psi_{t,i} \sin\beta_i = 0, \tag{2e}$$

$$I_{zv,i}\ddot{\theta}_{zv,i} + \gamma_i r_{v,i} k_{m,i}\delta_i \sin\psi_{t,i} \cos\beta_i = 0, \tag{2f}$$

$$\varepsilon = \begin{cases} +1, & \text{for } v = p, \\ -1, & \text{for } v = g. \end{cases} \tag{2g}$$

or in matrix form, $[M_i]\{\ddot{U}_i\} + [K_i]\{U_i\} = \{F_i\}$, where $i = 1, 2, \ldots, n$ refers to the mesh number and $\{U_i\} = \{\mathbf{u}_{p,i}^{\mathrm{T}}, \mathbf{u}_{g,i}^{\mathrm{T}}\}^{\mathrm{T}}$. In equation (2), $r_{p,i}$ and $r_{g,i}$ are the pitch circle radii of the pinion and gear, respectively, $k_{m,i}$ is the averaged mesh stiffness, k_b terms refer to the effective bearing stiffnesses, and γ_i is the rotational coefficient. For a clockwise rotating pinion, $\gamma_i = 1$, while for a counter-clockwise rotating pinion, $\gamma_i = -1$. Therefore, formulating γ_i into the above equations generalizes the theory because it can be used to describe the motions of successive meshes whose pinion rotation alternates from one direction to another consecutively, model asymmetric multi-mesh system, and simulate forward and reverse drive and coast operating conditions. The orthogonal projections of $\mathbf{u}_{p,i}$ and $\mathbf{u}_{g,i}$ onto the line of action normal to the tooth surface lead to the elastic deformation δ_i given as

$$\delta_i = \tau_{g,i} - \tau_{p,i} + e_i(t), \tag{3a}$$

$$\begin{aligned} \tau_{p,i} = {} & (\gamma_i u_{xp,i} + \gamma_i r_{p,i}\theta_{yp,i} \sin\beta_i - \gamma_i r_{p,i}\theta_{zp,i} \cos\beta_i) \sin\psi_{t,i} \\ & + (-u_{yp,i} \sin\alpha_i + u_{zp,i} \cos\alpha_i - \gamma_i r_{p,i}\theta_{xp,i} \cos\phi_{t,i}) \cos\psi_{t,i}, \end{aligned} \tag{3b}$$

$$\begin{aligned} \tau_{g,i} = {} & (\gamma_i u_{xg,i} - \gamma_i r_{g,i}\theta_{yg,i} \sin\beta_i + \gamma_i r_{g,i}\theta_{zg,i} \cos\beta_i) \sin\psi_{t,i} \\ & + (-u_{yg,i} \sin\alpha_i + u_{zg,i} \cos\alpha_i + \gamma_i r_{g,i}\theta_{xg,i} \cos\phi_{t,i}) \cos\psi_{t,i}. \end{aligned} \tag{3c}$$

From equation (3) above, δ_i can also be interpreted as the dynamic part of transmission error response. Hence, the dynamic mesh force is $F_{m,i} = k_{m,i}\delta_i$.

It follows that the universal multi-mesh geared rotor system model, expressed as the classical second-order proportionally damped differential equation in matrix form

$$[M]\{\ddot{U}\} + [C]\{\dot{U}\} + [K](U) = \{F\} \text{ for } \{U\} = \{\theta_{x,E} \ \{U_1\}^{\mathrm{T}} \ \{U_2\}^{\mathrm{T}} \ \cdots \ \{U_n\}^{\mathrm{T}} \ \theta_{x,L}\}^{\mathrm{T}},$$

is obtained by combining equations (2) and (3) of each gear pair with the dynamical expression of engine, load and counter-shaft components using a matrix superposition method. The governing equations for the engine with inertia I_E and load with inertia I_L are $I_E\theta_{x,E} + k_{\theta_{x,E}}(\theta_{x,E} - \theta_{xp,1}) = 0$ and $I_L\ddot{\theta}_{x,L} + k_{\theta_{x,L}}(\theta_{x,L} - \theta_{xg,n}) = 0$, respectively. For compliant counter-shaft, the Timoshenko beam theory [14] is used to formulate the stiffness matrix $[K^F_{s,i}]$ of two-noded shaft elements, $i = 1, 2, \ldots, n-1$. Note that $[K^F_{s,i}]$ and related forms are well studied [14–17]. A survey of these models indicated that the one developed by Przemieniecki [14] is most suitable for our analysis. The shaft mass and inertia terms are divided equally between adjacent gear centroids to limit the total number of system co-ordinates. The resulting mass $[M^F]$, stiffness $[K^F]$ and forcing $\{F^F\}$ terms assuming flexible shaft (superscript F) are

$$[M^F] = [M_G] + [M^F_s], \qquad [K^F] = [K_G] + [K^F_s], \qquad \{F^F\} = \{F_G\}, \qquad \text{(4a–c)}$$

where the first set of matrix terms on the right hand side of equation (4) denoted by subscript G contains contribution from gear pair, engine and load components. They are explicitly given by

$$[M_G] = [\mathrm{Diag}(I_E \quad [M_1] \quad [M_2] \quad \cdots \quad [M_n] \quad I_L), \tag{5a}$$

$$[K_G] = \begin{bmatrix} k_{\theta_{x,E}} & \{K_E\}^{\mathrm{T}} & & & & & & \\ \{K_E\} & [\tilde{K}_1] & & & & & & \\ & & [K_2] & & & & & \\ & & \ddots & & & & & \\ & & & [K_{n-1}] & & & & \\ & & & & [\tilde{K}_n] & \{K_L\} & & \\ & & & & \{K_L\}^{\mathrm{T}} & k_{\theta_{x,L}} & & \end{bmatrix}_{(12n+2)\times(12n+2)} \tag{5b}$$

$$\{F_G\} = \{0 \quad \{F_1\}^{\mathrm{T}} \quad (F_2)^{\mathrm{T}} \quad \cdots \quad \{F_n\}^{\mathrm{T}} \quad 0\}^{\mathrm{T}}. \tag{5c}$$

On the other hand, $[M^F_s]$ and $[K^F_s]$ define the cumulative mass and stiffness characteristics of the counter-shafts:

$$[M^F_s] = [\mathrm{Diag}(\{0\}_{1\times 7} \quad [m_{s,1}] \quad [I_{s,1}] \quad [m_{s,1}] \quad [I_{s,1}] \quad [m_{s,2}] \quad [I_{s,2}] \quad [m_{s,2}] \quad [I_{s,2}]$$
$$\cdots \quad [m_{s,n-1}] \quad [I_{s,n-1}] \quad \{0\}_{1\times 7})]_{(12n+2)\times(12n+2)}, \tag{6a}$$

$$[K_s^F] = \begin{bmatrix} [0]_{7\times 7} & & & & & \\ & [K_{s,1}^F] & & & & \\ & & [K_{s,2}^F] & & & \\ & & & \ddots & & \\ & & & & [K_{s,(n-1)}^F] & \\ & & & & & [0]_{7\times 7} \end{bmatrix}_{(12n+2)\times(12n+2)}, \tag{6b}$$

where $[m_{s,i}]$ and $[I_{s,i}]$ correspond to the mass and inertia of a counter-shaft half-length.

For a counter-shaft whose bending stiffness is high compared to k_m, a quasi-rigid body element representation (superscript R) is used to produce a simpler, lower order system model where the counter-shaft is elastic only in the u_x and θ_x directions. This mixed formulation is valid because the effect of cross-axis sensitivity is negligible. First, a partial system stiffness matrix $[\tilde{K}^R] = [K_G] + [K_C]$ is obtained by incorporating the axial and torsional matrix $[K_C]$ of counter-shafts with $[K_G]$ of the gear pairs. Similar to equation (6b), $[K_C]$ contains $n+1$ sub-matices denoted by $[\tilde{K}_{c,i}]$ as the diagonal terms, $i = 1, 2, \ldots, n+1$, in which the first ($i = 1$) and the last ($i = n+1$) ones are null matrices of dimension 7. The remaining $[\tilde{K}_{c,i}]$ is of dimension 12×12 and in fact quite sparse with non-zero terms given by $\tilde{K}_{c,i}(1,1) = \tilde{K}_{c,i}(7,7) = -\tilde{K}_{c,i}(1,7) = -\tilde{K}_{c,i}(7,1) = A_{s,i}E_{s,i}/L_{s,i}$ and $\tilde{K}_{c,i}(4,4) = \tilde{K}_{c,i}(10,10) = -\tilde{K}_{c,i}(4,10) = -\tilde{K}_{c,i}(10,4) = G_{s,i}J_{s,i}/L_{s,i}$, where $A_{s,i}$, $L_{s,i}$, $G_{s,i}$, $J_{s,i}$, and $E_{s,i}$ are the cross-sectional area, counter-shaft length, torsional rigidity, polar moment of inertia, and modulus of elasticity, respectively. The transverse bending effect is modelled by considering the kinematic equations for a rigid beam-like linkage:

$$u_{yg,i} = u_{ys,i} - \theta_{zs,i}L_{sa,i}, \qquad u_{yp,i+1} = u_{ys,i} + \theta_{zs,i}L_{sb,i}, \qquad \theta_{yg,i} = \theta_{yp,(i+1)} = \theta_{ys,i}, \tag{7a–c}$$

$$u_{zg,i} = u_{zs,i} + \theta_{ys,i}L_{sa,i}, \qquad u_{zp,i+1} = u_{zs,i} - \theta_{ys,i}L_{sb,i}, \qquad \theta_{zg,i} = \theta_{zp,(i+1)} = \theta_{zs,i}, \tag{7d–f}$$

where $L_{sa,i}$ and $L_{sb,i}$ are the distances between the counter-shaft centroid and its two attached gears. Hence, $L_{sa,i} + L_{sb,i} = L_{s,i}$.

Applying these kinematic constraints in the form of an orthogonalized transformation matrix $[T_{s,i}]$ reduces the independent coordinates to 50% by converting the original gear pair co-ordinates $\{\mathbf{u}_{g,i}^{\mathrm{T}}, \mathbf{u}_{p,i+1}^{\mathrm{T}}\}^{\mathrm{T}}$ to a new set of independent vectors $\{U_i^R\} = \{u_{xg,i}, \theta_{xg,i}, u_{ys,i}, u_{zs,i}, \theta_{ys,i}, \theta_{zs,i}, u_{xp,i+1}, \theta_{xp,i+1}\}^{\mathrm{T}}$ for $i = 1, 2, \ldots, n-1$:

$$\{\bar{\mathbf{u}}_{g,i}^{\mathrm{T}}, \mathbf{u}_{p,i+1}^{\mathrm{T}}{}^{\mathrm{T}}\}^{\mathrm{T}} = [\mathrm{T}_{s,i}]_{12\times 8}\{U_i^R\}. \tag{8}$$

The non-zero terms of $[T_{s,i}]$ are $T_{s,i}(2,6) = -L_{sa,i}$, $T_{s,i}(3,5) = L_{sa,i}$, $T_{s,i}(8,6) = L_{sb,i}$, $T_{s,i}(9,5) = -L_{sb,i}$, and the values of elements (1, 1), (2, 3), (3, 4), (4, 2), (5, 5), (6, 6), (7, 7), (8, 3), (9, 4), (10, 8), (11, 5) and (12, 6) are equal to unity. The overall transformation matrix $[T]$ has diagonal terms $[T_{s,i}]$ and converts $[\tilde{K}^R]$ into a new

system stiffness matrix $[K^R] = [T]^T[\tilde{K}^R][T]$ that is compatible with the diagonalized mass matrix $[M^R]$ from the lumped mass concept. Also, the corresponding force and response vectors are $\{F^R\} = [T]^T\{F_G\}$ and $\{U^R\} = \{\{U_0^R\}^T, \{U_1^R\}^T, \{U_2^R\}^T, \ldots, \{U_n^R\}^T\}^T$, respectively.

The solution of undamped natural frequencies and associated mode shapes is computed from the classical eigenvalue problem $([K] - \omega^2[M])\{\tilde{q}\} = \{0\}$ that is formulated by assuming a harmonic complex solution $\{u\} = \{\tilde{q}\}\exp(i\omega t)$. The system forced response is computable by the direct matrix inversion or modal expansion method. These solution techniques are based on established principles, and hence will not be discussed in detail here. However, it is worth noting that the forcing function $\{F_i\} = f(e_i)$ is general since the phasing of each e_i can be defined arbitrarily. Our formulation also allows a selective analysis for specific transmission error excitation. The damping effect is defined in terms of modal coefficients, which is covenient for the modal forced response calculation method. Therefore, in the direct matrix inversion scheme $[C] = ([Q]^T)^{-1}[\text{diag}(\zeta)][Q]^{-1}$, where the mode shape matrix $[Q]$ has been normalized with respect to $[M]$ to ensure compatability of both approaches. These calculations have been implemented using a general matrix computation program (MATLAB).

3. RESULTS AND VALIDATION

The two specific cases, i.e., $n = 2$ and 3, which are commonly used in multi-mesh applications, are analyzed to demonstrate the effectiveness of the proposed model. In the first case study for $n = 2$ and unity transmission ratio, our predictions are compared to the experimental data by Umezawa and his colleagues [13]. Note that $\gamma_i = 1$ ($\gamma_2 = -1$) and $\gamma_1 = -1$ ($\gamma_2 = 1$) formulations lead to the same modal behavior due to the symmetry of this system.

The primary torsional response peak of this system is measured at $f_T = 2300$ Hz, which is similar to the theoretical torsional mode with out-of-phase mesh

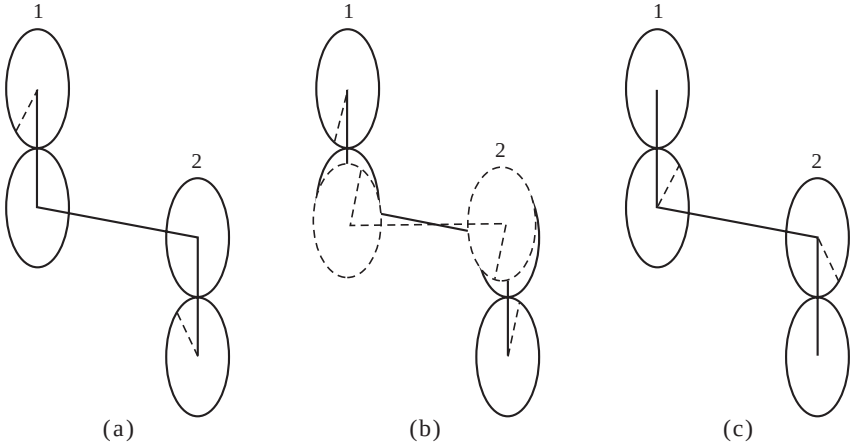

Figure 3. Critical modes of the dual-mesh counter-shaft geared rotory system: (a) mode A ($f_n = 2271$ Hz): out-of-phase torsion; (b) mode B ($f_n = 7180$ Hz): counter-shaft pitch; and (c) mode C ($f_n = 36{\cdot}82$ kHz): counter-shaft torsion.

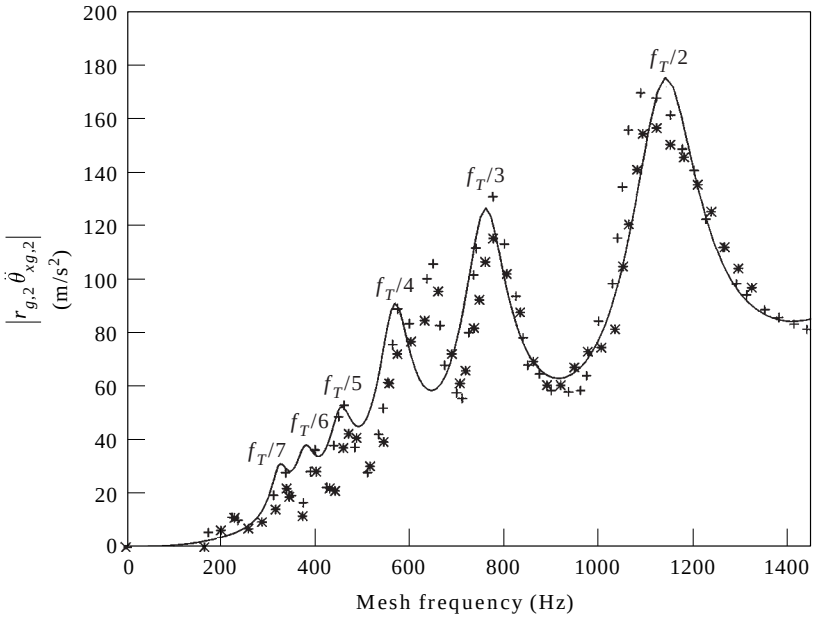

Figure 4. Comparison of predicted and measured frequency sweep forced response functions of the output gear ($r_{g,2}\ddot{\theta}_{xg,2}$) for the case of $n = 2$. Keys: —, prediction; +, measurement (set 1); *, measurement (set 2).

deflections at 2271 Hz as shown in Figure 3, along with two other critical gear mesh modes. These results are also confirmed by the finite element calculation. Figure 4 shows relatively good comparison (except for a spurious peak between

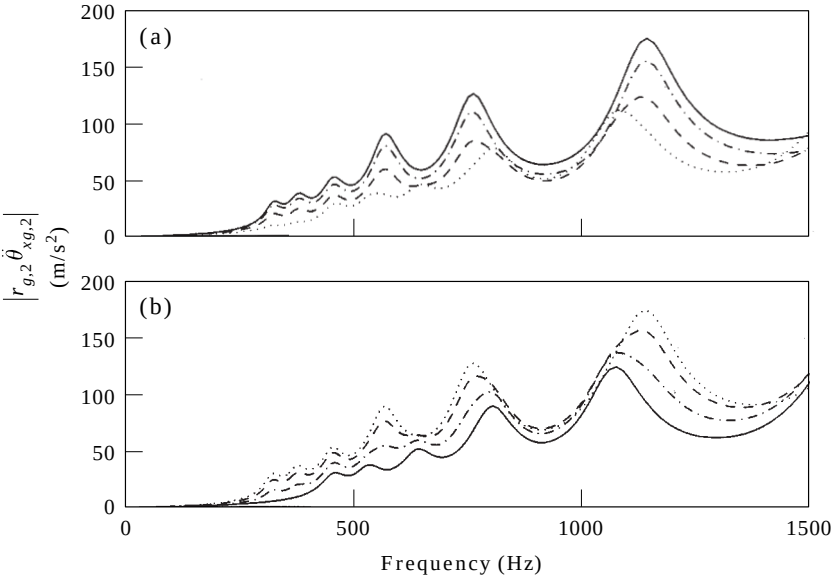

Figure 5. Effect of relative phasing of transmission error $\Phi_{2,k}$ on vibratory response of output gear ($r_{g,2}\ddot{\theta}_{xg,2}$) for counter-shaft length $L_s = 190$ mm: (a) —, 0°; –·–, 45°; – – –, 90°; · · · · ·, 135°; (b) —, 180°; –·–, 225°; – – –, 270°; · · · · ·, 315°.

TABLE 1

Qualitative classification of flexible modes in terms of gear pair location 1, 2 *and* 3 *for* $n = 3$. *Note that out-of-phase type motions are given in* ( ), *and the others are assumed in-phase*

n	F_n(Hz)	u_x	u_y, u_z	θ_x	θ_y, θ_z
6	2·77			(3)	(1), (3)
7	6·06			1, 2, 3	(1)
8	262			1, 3	(1), (3)
9	402			1, 2, 3	(1), (3)
10	1428		(2), (3)	(2), (3)	2, (3)
11	1642		(2), (3)	(2), (3)	(2), (3)
12	1686		(2), 3	(2), (3)	(2), (3)
13	1803		(1)	(1)	(1), (2)
14	1972	(2), 3	(1), 2, (3)	(1), (2), (3)	(1), (2), 3
15	2043	(2), (3)	(1), 2, (3)	(2)	(1), (2)
16	2128		(1), 2, (3)	(2)	(1), (2)
17	2193		(2), (3)		(2), (3)
18	2336	(1), (2), 3	2, (3)	(1), (3)	(1), 2, (3)
19	2361	(1), (2)	(1), (2)	(1), (2)	(1), (2)
20	2428	(1), (2)	(1), (2)	(1)	(1), (2)
21	2578	(3)	(3)		
22	2578	(3)	(3)		
23	2598	1, (2)	1, (2)	(1)	1, (2)
24	3040		(2)	(2)	(1), 2
25	3196	(3)	(3)	(2), (3)	(2), (3)
26	2246	(1)	(1)		
27	3346	(1)	(1)		
28	3941	(1)	(1)	(1)	(1)
29	4438	(2), (3)			
30	5046	(1), (2)			

$f_T/4$ and $f_T/3$, and a slight shift of the $f_T/2$ peak) of predicted and measured frequency sweep forced response functions of the output gear in terms of $|r_{g,2}\ddot{\theta}_{xg,2}|$ due to exact in-phase transmission error excitations. These minor discrepancies are probably attributed to non-linearity in the system and effect of damping on f_T, which are not directly considered here and beyond the scope of this study. The models of e_1 and e_2 are semi-empirical and consist of seven significant mesh harmonics expressed as $e_i = \Sigma_{k=1}^{7} e_{i,k} \exp(jk\omega t + \Phi_{i,k})$ for $i = 1, 2$ to adequately fill the operating speed and frequency ranges. Since each mesh harmonic is assumed incoherent, the total mean square response is given by

$$\{|U|\} = \left\{\sqrt{\sum_{k=1}^{7} |U_k|^2}\right\},$$

where $|\ddot{\theta}_{xg,2}(\omega)| = \omega^2 |U(17)|$.

The effect of tooth mesh phase lag is analyzed and shown in Figure 5 as it was also discussed in reference [13]. This is simulated by varying $\phi_{2,k}$, the phase of e_2

relative to e_1. Since the system mass and stiffness distributions remain invariant, the basic modal behavior stays like the baseline result. However, the forced response varies with $\Phi_{2,k}$, due to a shift in the relative contribution of e_1 and e_2. As $\Phi_{2,k}$ is varied from 0 to 180° at increments of 45°, the dynamic responses decrease monotonically. For 180 to 360°, the responses rise steadily back to the original level. Also, the specific system mode excited by e_i is dependent on the angular quadrant of $\Phi_{2,k}$. For instance, the resonance peak at $f_T/2 \cong 1180$ Hz disappear for the $\Phi_{2,k} = 135°$ case and is displaced by $\tilde{f}_T/3 \cong 1070$ Hz that corresponds to a different torsional mode at $\tilde{f}_T$. In general, f_T is the dominant natural frequency when $\Phi_{2,k}$ ranges from -90 to 90°, while $\tilde{f}_T$ becomes the primary resonance when $\Phi_{2,k}$ is between 90 and 270°.

To further demonstrate the capability of the proposed model, a tri-helical mesh counter-shaft speed reducer with transmission ratio equal to 2:1 is considered next. The analytical model assumes quasi-rigid shaft and possesses 30 independent co-ordinates. The eigenvalue analysis produces five rigid body and 25 flexible modes. Their natural frequencies are within $\pm 3\%$ discrepancy of finite element calculations. The flexible modes are classified according to their basic characteristics of relative transverse, torsion and coupled rotation-translation modal behavior, as described in Table 1. Here, a specific characteristic is considered significant when its corresponding eigenvector term $\tilde{q}_{n,j}$ satisfies $\tilde{q}_{n,j}/\tilde{q}_{n,max} \geqslant 0{\cdot}1$, where $\tilde{q}_{n,max}$ is the highest relative term in $\{\tilde{q}_n\}$. The dynamic mesh forced response $F_{m,i}$ per harmonic excitation e_i of this $n = 3$ model for $\gamma_1 = 1$ (solid line) and $\gamma_1 = -1$ (dashed line) conditions are shown in Figure 6. The results show

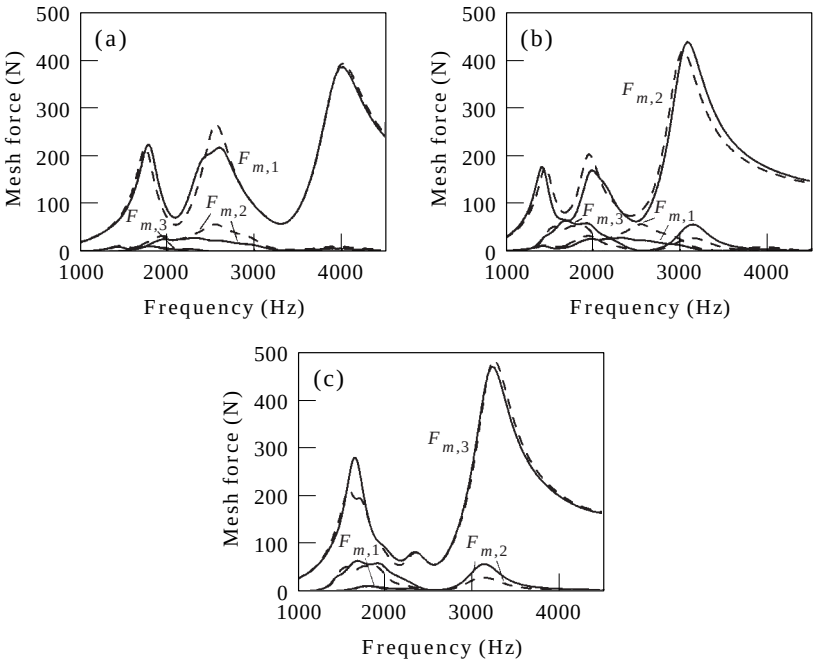

Figure 6. Mesh force response $F_{m,i}$ due to fundamental harmonic of e_i applied individually: (a) e_1, (b) e_2, (c) e_3. Keys: —, $\gamma_1 = 1$; ----, $\gamma_1 = -1$.

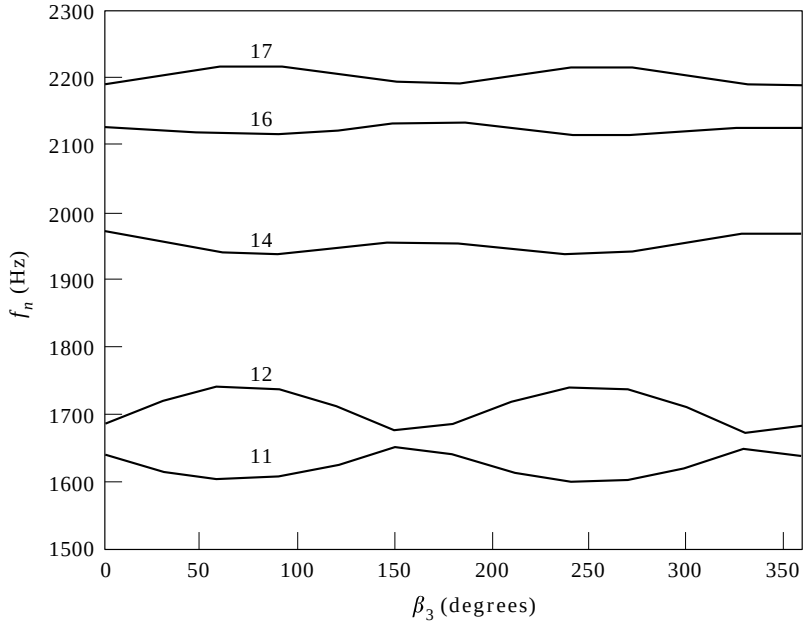

Figure 7. Effect of β_3 on selected f_n for $n = 3$.

the majority of the resonant peaks occur within the range of 1–4 kHz and are due to modes with significant torsional and translational coupling as depicted qualitatively in Table 1. Note the dissimilarities between the responses of different gear pairs. For example, $F_{m,1}(\omega)/e_1$ contains the response from modes 13, 19, 20 and 23, and $F_{m,2}(\omega)/e_2$ is controlled by modes 10, 14, 15 and 24, while only modes 11, 12, 18 and 25 are being excited in $F_{m,3}(\omega)/e_3$. Also, the presence of helical gears create a slight asymmetry. Hence, the response is affected by the operating conditions related to rotational directions and coast/drive arrangements.

Finally we use the proposed formulation of the $n = 3$ model to evaluate the effect of gear pair position angle β on f_n and the dynamic response. By varying β, an assorted number of transmission layouts can be evaluated quickly, which is equivalent to analyzing a large number of preliminary designs at the conceptual stage. Figure 7 shows the results of f_n when varying β_3 and keeping $\beta_1 = \beta_2 = 0$. The lower ($f_n < 1500$ Hz) and higher ($f_n > 2300$ Hz) sets of natural frequencies are virtually unaffected by β_3. However, the modes in the range of 1500–2300 Hz are found to vary periodically with periodicity of 360°. The amplitude of the variation Δf_n is almost up to 50 Hz.

Next, β_2 and β_3 are varied systematically from 0 to 360° to study their composite effects on overall dynamic response. Mapping the effects of β_2 and β_3 simultaneously produces results for all possible configuration of the $n = 3$ case. To evaluate the massive amount of calculated data in a compact form, only the maximum mesh force peak response of $F^*_{m,i}(\omega)$ and total mesh power $P_m = \Sigma_{i=1}^{3} \int F_{m,i}\delta_i \, \mathrm{d}f$ from 1 to 3 kHz that encompasses the majority of the dynamics are examined, as shown in Figures 8 and 9, respectively. The 3-D topographical curves and the corresponding 2-D contour plots produce highly

structured dynamic characteristics. The specific regions of local maximum and minimum in $F^*_{m,i}(\beta_2, \beta_3)$, $P_{m,i}(\beta_2, \beta_3)$ and $P_m(\beta_2, \beta_3)$ are quite similar. Their degree of steepness (directly proportional to the density of the contour lines) gives an indication of the sensitivity of a particular configuration. For instance, $P_{m,1}$ and $F^*_{m,1}$ are found to be sensitive to slight perturbation in β_2 for $200^\circ < \beta_2 < 300^\circ$, where they are also maximum. In contrast, they are virtually insensitive to β_3 for any value of β_2. Further examination of the 2-D contour patterns reveals three types of equi-magnitude lines. One set is aligned with the axes of β_3 while another set makes a 45° angle. The third kind is nearly elliptical in shape with its major axis oriented approximately at a 45° angle. The first-type of equi-magnitude horizontal lines appear in $F^*_{m,1}$ and $P_{m,1}$ functions primarily because they are not affected much by β_3. The second type is seen in $F^*_{m,3}$ and $P_{m,3}$ whose contour lines

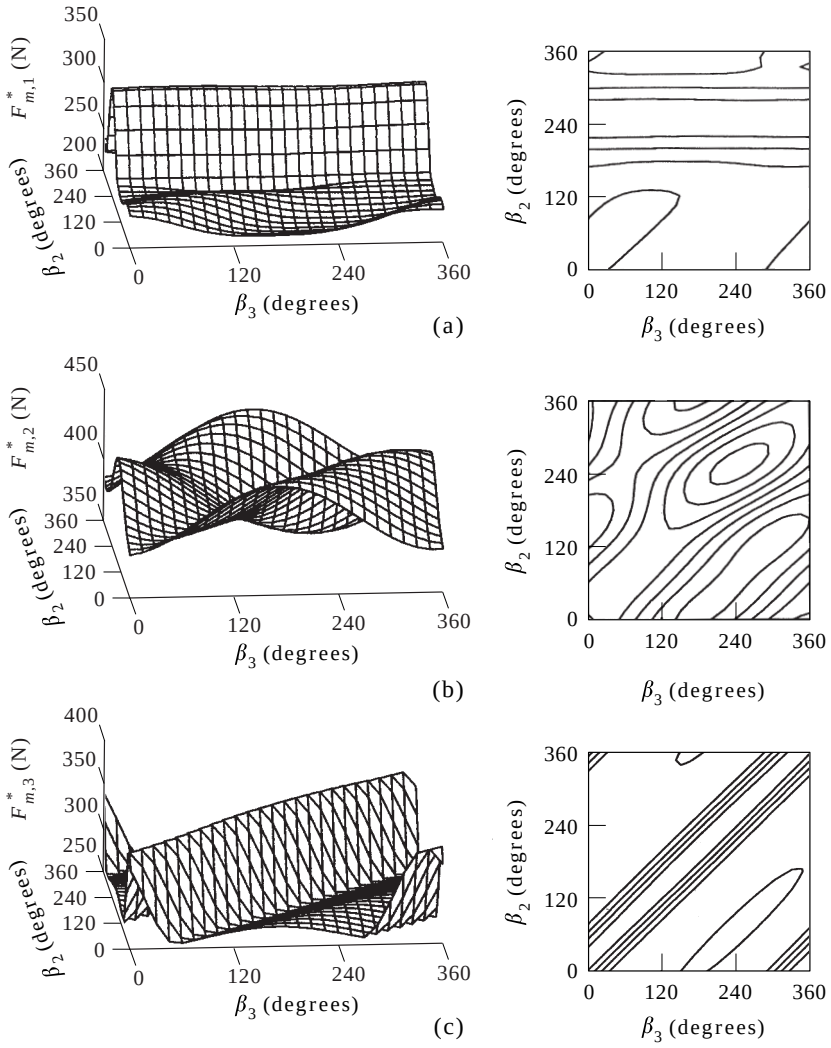

Figure 8. Maximum mesh force peak F^*_m topographical and contour plots as a function of β_2 and β_3 for $n = 3$: (a) $F^*_{m,1}$, (b) $F^*_{m,2}$, (c) $F^*_{m,3}$.

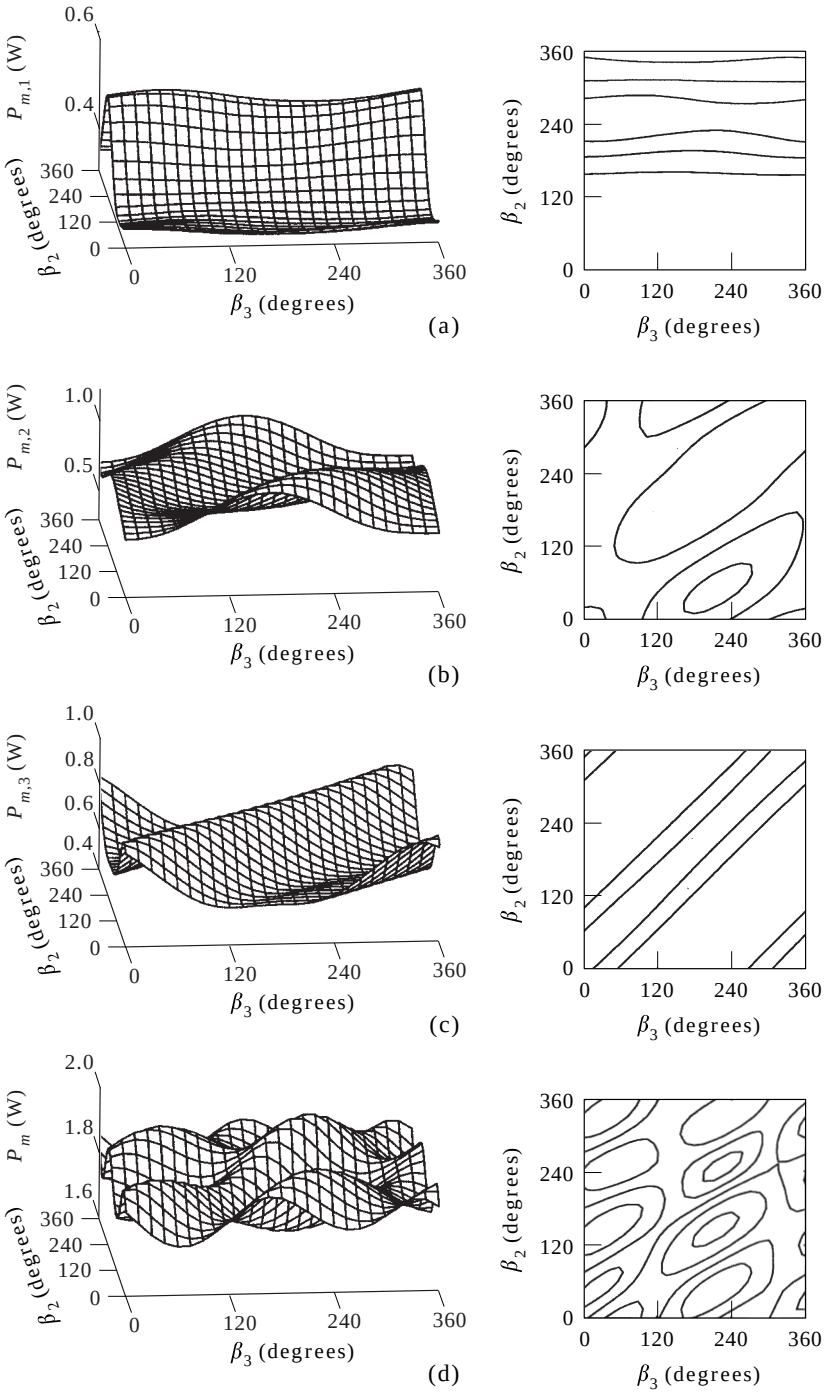

Figure 9. Mesh power P_m topographical and contour plots as a function of β_2 and β_3 for $n = 3$: (a) $P_{m,1}$, (b) $P_{m,2}$, (c) $P_{m,3}$, (d) P_m.

can be generalized by $\beta_2 - \beta_3 = \text{constant}$. This condition reflects the invariant dynamic behavior of $F^*_{m,3}$ and $P_{m,3}$, as long as the same angular position between the second and third gear pairs is maintained. The elliptical trend is seen mostly in $F^*_{m,2}$, $P_{m,2}$ and P_m. These elliptical curves imply that the dynamics of the second mesh is affected by both $\beta_2 - \beta_1$ and $\beta_3 - \beta_2$, while the other two meshes are influenced only by either $\beta_2 - \beta_1$ or $\beta_3 - \beta_2$ but not both. Also note that the specific features of these equi-magnitude lines are somewhat dependent on the choice of the reference position angle. Suppose β_3 is the reference position angle where $\beta_3 = 0$ instead of $\beta_1 = 0$, the orientations of the straight equi-magnitude lines of $F^*_{m,1}$, $P_{m,1}$, $F^*_{m,3}$ and $P_{m,3}$ will change. The contour plots (β_1 versus β_2) of $F^*_{m,1}$ and $P_{m,1}$ is expected to show 45° lines while the ones associated with $F^*_{m,3}$, and $P_{m,3}$ will produce vertical lines that are parallel to the β_1 axis. The contours of $F^*_{m,2}$, $P_{m,2}$ and P_m will still remain elliptical. On the other hand, if β_2 is used as the reference ($\beta_2 = 0$), the contours of $F^*_{m,1}$, $P_{m,1}$, $F^*_{m,3}$ and $P_{m,3}$ will generate equi-magnitude lines that are perpendicular to the axes of their own position angle. Again, the contours of $F^*_{m,2}$, $P_{m,2}$ and P_m will depict elliptical trends.

Similarly, other combinations of response variables and design parameters can be computed easily and evaluated systematically. Even though limited results are shown here, the proposed formulation is shown to be reasonably accurate and highly useful for computing the dynamic response of a n-mesh counter-shaft geared rotor system. It is especially adaptable to study a large number of geomerical configurations and parametric effects, which are suitable for evaluating preliminary designs where detailed demensions are still undefined.

REFERENCES

1. H. Ozguven and D. R. Houser 1988 *Journal of Sound and Vibration* **121**, 83–411. Mathematical models used in gear dynamics—a review.
2. G. W. Blankenship and R. Singh 1992 *Proceedings of Sixth International Power Transmission and Gearing Conference*, DE 43-1, 137–146. A comparative study of selected gear mesh interface dynamic models.
3. H. Iida and A. Tamura 1984 *Proceedings of Vibration in Rotating Machinery*, 67–72. Coupled torsional–flexural vibration of a shaft in a geared system.
4. H. Iida, A. Tamura and M. Oonishi 1985 *Bulletin of the Japan Society of Mechanical Engineers* **28**, 2694–2699. Coupled torsional–flexural vibration of a shaft in a geared system (3rd report, Dynamic characteristics of a counter shaft in a gear train system).
5. H. Iida, A. Tamura and H. Yamamoto 1986 *Bulletin of the Japan Society of Mechanical Engineers* **29**, 1811–1816. Dynamic characteristics of a gear train system with softly supported shafts.
6. T. C. Lim and D. R. Houser 1997 *Proceedings of SAE Noise and Vibration Conference*, 739–749. Dynamic analysis of layshaft gears in automotive transmission.
7. A. Kahraman 1992 *Proceedings of Sixth International Power Transmission and Gearing Conference*, DE 43-1, 365–373. Dynamic analysis of a multi-mesh helical gear train.
8. H. Vinayak, R. Singh and C. Padmanabhan 1995 *Journal of Sound and Vibration* **185**, 1–32. Linear dynamic analysis of multi-mesh transmissions containing external, rigid gears.
9. H. Vinayak 1995 Ph.D. dissertation, The Ohio State University. Multi-body dynamics and modal analysis approaches for multi-mesh transmissions with compliant gear bodies.

10. G. W. Blankenship and R. Singh 1995 *Mechanism and Machine Theory* **30**, 43–57. A new gear interface dynamic model to predict multi-dimensional force coupling and excitation.
11. P. Velex and A. Saada 1991 *Proceedings of Eighth World Congress on the Theory of Machines and Mechanisms*, 26–31. A model for the dynamic behavior of multistage geared system.
12. F. K. Choy, Y. K. Tu, M. Savage and D. P. Townsend 1989 *Proceedings of the ASME International Conference on Gearing and Power Transmission*, 383–387. Vibration signature analysis of multi-stage gear transmission.
13. K. Umezawa, T. Ajima and H. Houjoh 1986 *Bulletin of Japan Society of Mechanical Engineers* **29**, 950–957. Vibration of three axes gear system.
14. J. S. Przemieniecki 1968 *Theory of Matrix Structural Analysis*. New York: McGraw-Hill.
15. J. S. Archer 1965 *American Institute of Aeronautics and Astronautics Journal* **3**, 1910–1918. Consistent matrix formulations for structural analysis using finite-element techniques.
16. W. Wang and W. D. Pilkey 1994 *The International Journal of Analytical and Experimental Analysis* **9**, 218–226. The exact frequency-dependent stiffness and mass matrices of a general beam element with axial force and flexible foundation.
17. T. Yokoyama 1990 *Journal of Sound and Vibration* **141**, 245–258. Vibrations of a hanging Timoshenko beam under gravity.